Temporal Decorrelation: A Theory of Lagged and Nonlagged Responses in the Lateral Geniculate Nucleus

Dawei W. Dong and Joseph J. Atick

Computational Neuroscience Laboratory
The Rockefeller University
1230 York Avenue
New York, NY 10021-6399

(*Network: Computation in Neural Systems* Vol 6(2) pp 159-178)

Abstract

Natural time-varying images possess significant temporal correlations when sampled frame by frame by the photoreceptors. These correlations persist even after retinal processing and hence, under natural activation conditions, the signal sent to the lateral geniculate nucleus is temporally redundant or inefficient. We explore the hypothesis that the LGN is concerned, among other things, with improving efficiency of visual representation through active temporal decorrelation of the retinal signal much in the same way that the retina improves efficiency by spatially decorrelating incoming images. Using some recently measured statistical properties of time-varying images, we predict the spatio-temporal receptive fields that achieve this decorrelation. It is shown that, because of neuronal nonlinearities, temporal decorrelation requires two response types, the *lagged* and *nonlagged*, just as spatial decorrelation requires *on* and *off* response types. The tuning and response properties of the predicted LGN cells compare quantitatively well with what is observed in recent physiological experiments.

Introduction

All retinal ganglion cells project heavily to the lateral geniculate nucleus, or LGN. With few exceptions, each geniculate cell receives its innervation from a single or a few retinal ganglion cells of the same class, and the spatial response properties of these geniculate neurons are essentially the same as those of their retinal counterparts with closely overlapping receptive fields (Hubel and Wiesel 1961; Singer and Creutzfeldt 1970; Cleland *et al.* 1971, So and Shapley 1979). Until recent years, it was commonly assumed that there is no significant receptive field transformation in the relay of retinal information to the cortex through the LGN.

However, if one examines the temporal aspects of retinal and LGN cell responses, there are some important differences for a wide range of operating conditions. The response of the LGN cells is much more transient than the ganglion cells, and their firing rates are lower; the LGN cells also perform a sharper temporal bandpass filtering of the incoming signal (Kaplan and Shapley 1982; Levine and Troy 1986). In addition, it has become clear recently that there could be two functional classes of LGN cells that differ in the phase of their temporal response: the lagged and nonlagged cells; the lagged cells have no counter part among retinal ganglion cells (Mastronarde 1987a,b; Saul and Humphrey 1990; Hartveit 1992). These observations, among others, confirm that the LGN is a computationally rich and exciting area to study. It is also an area that we believe is likely to be understood — just like the retina and primary visual cortex — from first principles of information processing since it is a relatively early stage in the visual pathway. In this paper we have taken a first step in this direction by proposing a quantitative theory of the LGN based on the principle of efficient coding.*

Earlier, it was proposed that the purpose of retinal processing is to improve the efficiency of visual representation by recoding the input into a spatially decorrelated form (Atick and Redlich 1990, 1992). This hypothesis was shown to lead to a quantitative theory of retinal processing that predicts spatio-chromatic receptive fields of ganglion cells that compare well with experimental data for the entire range of adaptation levels (Atick and Redlich 1992; Atick *et al.* 1992). In other works, the decorrelation dynamics (Dong 1993a,b) of lateral interaction between orientation selective cells in the early visual cortex was shown to yield quantitative predictions about orientation contrast, adaptation, and development of orientation selectivity which are in good agreement with experiments (Dong 1993b, 1994). It

*This principle states that the purpose of early sensory processing is to recode incoming signals into a redundancy reduced or efficient representation (Attneave 1954; Barlow 1961; Linsker 1989; Atick and Redlich 1990; Atick 1992a,b). The advantages of efficiency of information representation in the nervous system are numerous and they include dynamic range savings as well as cognitive advantages. What is most interesting about this principle is that it is predictive: given a source of inefficiency in an input signal (*e.g.* pairwise correlations) one predicts mathematical transforms that eliminate this inefficiency (*e.g.* decorrelate), and these can then be compared with the signal transformations observed in real experiments.

was also shown to account well for cortical color adaptation and binocular coding (Atick *et al.* 1993; Li and Atick 1994). However, all sources of inefficiency explicitly considered thus far are related to spatial correlations or correlations between different cells. What about correlations in the time domain or more generally spatio-temporal correlations?

In natural time-varying images, temporal correlations are very significant. It is compelling to believe that the visual pathway tries to improve efficiency by eliminating temporal correlations just like it seems to do with spatial correlations. Computationally, this process in time is more complex than in space. This may account for the fact that while the retina performs excellent spatial decorrelation, it does not do a good job in the temporal domain, which means that signals from the retina still contain excess temporal correlations. This leads us to the proposal that one of the main purposes of the LGN processing is to complete the temporal decorrelation of the retinal signal. We derive the spatio-temporal receptive fields (impulse response) for LGN cells based on this theory and show that the predicted tuning curves and response properties compare very well with the data of Saul and Humphrey (1990). Taking into account the hardware restriction of nonlinearity of real neurons (rectification), our analysis predicts four functionally distinct LGN cell classes lagged and nonlagged, on and off-center cells.

These results have been presented previously in abstract form (Dong and Atick, 1994a).

Methods

1. Receptive Fields from Efficient Coding: Linear case.

To code efficiently in the regime of high signal to noise, images must first be transformed into a representation where pixels are as statistically independent from each other as possible (factorial representation) (Barlow 1989; Atick 1992b). The dominant source of statistical dependence in natural visual input is due to pairwise pixel correlations (Field 1987; Hancock *et al.* 1992; Ruderman and Bialek 1994) and inter-frame correlations (Dong and Atick 1995). Nearby pixels in space and time in natural time-varying images tend to be very similar in their visual appearance, giving a luminosity profile which changes gradually in space-time and only abruptly at edges or motion ridges. Finding a more efficient representation — where correlations are absent — is tantamount to discovering the "visual vocabulary" that most compactly describes the world. What is interesting is that this vocabulary is predictable from measured properties of natural time-varying images.

We begin by mathematically formulating the problem of spatio-temporal decorrelation in the linear approximation. This means that the input signal $S(\underline{x}', t')$ — which is given by the photoreceptor activity at position $\underline{x}'$ on the retina and at time t' — is assumed to be linearly transformed to produce the LGN output signal $O(\underline{x}, t)$. Of course, real LGN cells are not linear and, in fact, as we shall see below, it is when we take the nonlinearities correctly into account that we discover a diversity in their temporal properties. However, much can

be learned from the linear approximation since above threshold and below saturation the response of many LGN cells is well approximated by a linear function. Also, after we derive some interesting predictions from the linear analysis we shall use the results as building blocks to arrive at the nonlinear LGN code.

1.1 Spatio-temporal decorrelation & temporal tuning

With the assumption of linearity

$$\begin{aligned} O(\underline{x},t) &= \int d\underline{x}'dt'\ K(\underline{x},\underline{x}';t,t')S(\underline{x}',t'), \\ &\equiv \mathbf{K}\cdot\mathbf{S}, \end{aligned} \tag{1}$$

where $\mathbf{K} \equiv K(\underline{x},\underline{x}';t,t')$ is the spatio-temporal kernel or receptive field and $\cdot$ denotes spatio-temporal convolution as defined above. The output $O(\underline{x},t)$ is directly related to the firing frequency of a cell in spikes/sec. This is a good characterization of the temporal response of spiking LGN cells since the time scales of their kernels are relatively long (hundreds of milliseconds) in comparison with the interspike time interval (several milliseconds).

The input signal $S(\underline{x}',t')$ possesses pairwise correlations captured by the spatio-temporal correlation matrix:

$$R(\underline{x},\underline{x}';t,t') =< S(\underline{x},t)S(\underline{x}',t') >, \tag{2}$$

in which brackets denote ensemble averaging. For the output to be decorrelated, *i.e.* activities of cells at different positions and time are uncorrelated, the transformation $\mathbf{K}$ must be chosen so as to achieve:

$$< O(\underline{x},t)O(\underline{x}',t') >= \delta(\underline{x}-\underline{x}',t-t'), \tag{3}$$

where $\delta(\underline{x},t)$ is the Kronecker delta function which is zero everywhere except for $\underline{x}=0$ and $t=0$ and is normalized to 1. Substituting (1) into (3) we get, in matrix notation, the following equation for the decorrelating transform $\mathbf{K}$

$$\mathbf{K}\cdot\mathbf{R}\cdot\mathbf{K}^T = \mathbf{1}. \tag{4}$$

Assuming translation invariance, *i.e.*, $K(\underline{x},\underline{x}';t,t') = K(\underline{x}-\underline{x}',t-t')$ and $R(\underline{x},\underline{x}';t,t') = R(\underline{x}-\underline{x}',t-t')$ — which is a reasonable approximation for foveal vision and is generally true for natural time-varying images— equation (4) can be rewritten in Fourier space as

$$K(\underline{f},w)\ R(\underline{f},w)\ K^*(\underline{f},w) = 1, \tag{5}$$

in which $\underline{f}$ and w are the spatial wave vector and temporal frequency, respectively, and * denotes complex conjugation. $K(\underline{f},w)$ is the *spatio-temporal* filter and $R(\underline{f},w)$ is the so-called *power spectrum* of time varying-images, and they are simply the Fourier transforms of $K(\underline{x},t)$ and $R(\underline{x},t)$, respectively. The modulus of the solution to equation (5) is simply

$$|K(\underline{f},w)| = \frac{1}{\sqrt{R(\underline{f},w)}}. \tag{6}$$

In a linear system, this modulus is proportional to the cell's response to a sinewave of spatial frequency $\underline{f}$ modulated at temporal frequency w. This cell produces an output whose power spectrum, in response to natural time-varying images, is flat or "white" ($|O(\underline{f}, w)|^2 = |K(\underline{f}, w)|^2 R(\underline{f}, w) = 1$). Equation (6) predicts the spatio-temporal frequency tuning if $R(\underline{f}, w)$ is known.

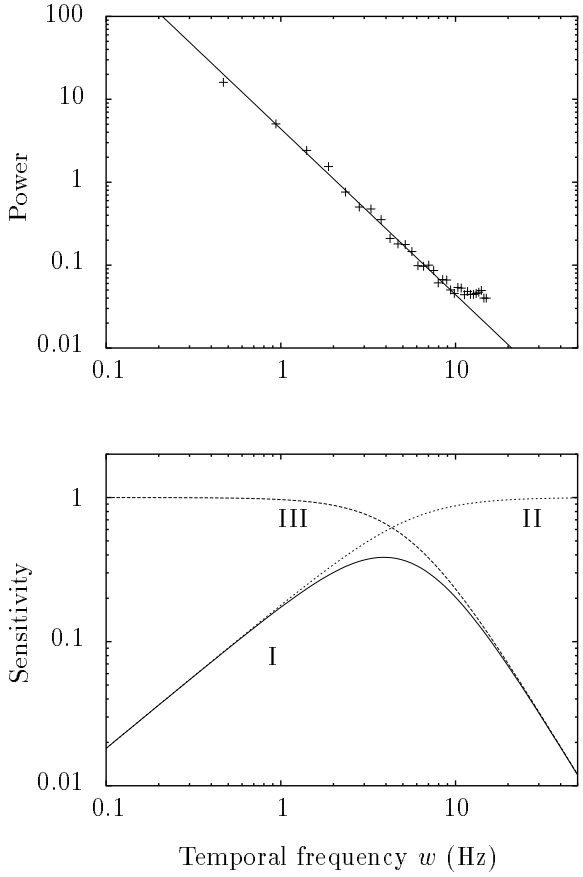

Figure 1: *top*: Measured temporal power spectrum of natural time-varying images from Dong and Atick (1995) showing that $R(0, w) \sim 1/w^2$ (solid curve) is a good approximation to the spectrum at low spatial frequencies. The value of this power spectrum is relative. The value in the space-time domain, which is of the correlation matrix, illustrates how strong the correlation is: in our measurements on 8-bits gray scale time-varying images, the correlation of a pixel, for example, slowly decreases from 2×10^3 at $t = 0$ (corresponding to standard deviation of 45) to 1×10^3 at $t = 1$ second. *bottom*: Predicted LGN temporal filter (curve I) which, in the low frequency regime, is given by $R(0, w)^{-\frac{1}{2}}$ (curve II) while at high frequency asymptotes the lowpass filter (curve III) which suppresses noise ($w_c = 5.5$ Hz).

$R(\underline{f}, w)$ was recently measured by Dong and Atick (1995). These measurements (see Figure 1-top) show that in the limit $\underline{f} \to 0$, $R(0, w)$ reduces to

$$R(0, w) \sim \frac{1}{w^2}. \tag{7}$$

This immediately predicts:

$$|K(0,w)| = \frac{1}{\sqrt{R(0,w)}} \sim w. \tag{8}$$

The data on typical LGN neurons supports the presence of a linear regime at high light level and at low temporal frequency (Saul and Humphrey 1990).†

To quantitatively compare our predictions with available experimental data we need to take noise into account, since in reality the input includes not only the signal S but also some noise N. The filter K derived above applies to and decorrelates both the signal and noise

$$|K(\underline{f},w)| = \frac{1}{\sqrt{R}} = \frac{1}{\sqrt{S^2(\underline{f},w)+N^2}}, \tag{9}$$

in which $S^2(\underline{f},w)$ is the power spectrum of the signal and N^2 is the noise power. At high temporal frequency and at low light level the noise is significant and this whitening filter will magnify noise relative to the signal. To code efficiently in the presence of noise, a lowpass filter is needed, in addition to decorrelation, to guarantee that no significant noise is passed to the output: *i.e.*, "smoothing" when noise is significant and decorrelation when the signal to noise ratio is high. Both smoothing and decorrelation contribute to efficiency, since they compress the signal by eliminating noise and correlations, respectively. ‡ The simplest smoothing filter is the so-called Wiener filter (Press *et al.* 1988), which is the filter M which when applied to the corrupted signal, $K(S+N)$, produces a signal that is as close as possible to KS, where "close" is measured in the least-square sense, *i.e.*,

$$\chi^2 = \int d\underline{f}dw|MK(S+N) - KS|^2 \tag{10}$$

is minimized. It is straight forward to show that the optimal noise suppressing solution $\delta\chi^2/\delta M = 0$ is

$$M = \frac{S^2}{S^2+N^2} = \frac{R-N^2}{R}. \tag{11}$$

This smoothing filter approaches zero at high noise level and one at low noise level.

†Our measurements also confirm the power spectrum of snap-shot images first measured by Field (1987) who discovered that $R(\underline{f}) \sim \frac{1}{|\underline{f}|^2}$, which led to the prediction that the spatial contrast sensitivity (in the regime where noise can be ignored) of ganglion cells (or equivalently of LGN cells) is $|K(\underline{f})| \sim |\underline{f}|$ (Atick and Redlich 1992).

‡The principle of efficient coding in the presence of noise has been formulated carefully in (Atick and Redlich 1990), where the smoothing and decorrelation processes are shown to be two limits of optimization of the mutual information of the output relative to the pure input signal subject to certain constraints. It was further shown, that — contrary to the decorrelating filter — the smoothing filter predicted depends on the details of the constraints imposed. The precise set of constraints is not clear at the moment and hence the details of the lowpass filter are somewhat flexible. However, as long as the lowpass filter has a proper cut-off frequency, the detailed form of it does not change the final result significantly. That is why we leave the cut-off frequency as a free parameter, which is the only parameter in our theory.

So taking noise into consideration, we predict that the spatio-temporal LGN filter in the linear regime is the product of the decorrelation filter and the smoothing filter:

$$|K(\underline{f}, w)| = \frac{1}{\sqrt{R}} M = \frac{1}{\sqrt{R}} \frac{R - N^2}{R}. \tag{12}$$

To exhibit the temporal behavior of this filter explicitly we need an explicit expression of the noise.

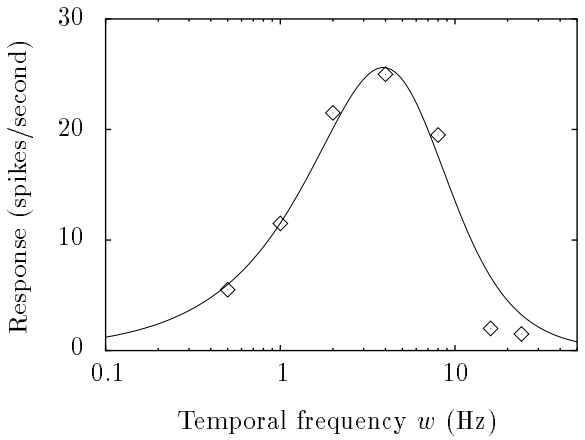

Figure 2: Comparison between predicted temporal tuning curve (solid curve) and LGN data (diamonds) from a typical cell as measured by Saul and Humphrey (1990). The predicted curve is generated from equation (14) with $w_c = 5.5$ Hz.

We assume the noise is temporal white noise, thus in the presence of noise,

$$R(w) \sim \frac{1}{w^2} + \frac{1}{w_c^2}, \tag{13}$$

for some characteristic noise frequency w_c. Substituting (13) into (12) we finally predict:

$$|K(w)| \sim \frac{w}{(1 + w^2/w_c^2)^{\frac{3}{2}}}, \tag{14}$$

valid for all w. We have plotted this filter in Figure 1-bottom, curve I. At low frequency it is completely determined by the power spectrum of natural time-varying images and is linear in w (curve II); at high frequency it asymptotes the smoothing filter (curve III) and cuts off as the noise becomes significant. In Figure 2 we have superimposed the temporal tuning data of a typical cat LGN cell from Saul and Humphrey (1990) on our predicted filter, equation (14). The noise cutoff w_c is the only parameter in (14), the curve plotted is for $w_c = 5.5$ Hz, which shows remarkable quantitative agreement with the experimental data.

1.2 Spatio-temporal Receptive Fields

To predict the receptive fields we need to determine not only the modulus of the solution, $|K(\underline{f}, w)|$, but also the phase before we can Fourier transform back to space-time. The problem is that the decorrelation condition, equation (5), determines the solution only up to an a priori arbitrary phase $\Phi(\underline{f}, w)$. Since given a solution $K(\underline{f}, w)$, we can always construct another decorrelating solution $K(\underline{f}, w)' = e^{i\Phi(\underline{f},w)}K(\underline{f}, w)$, which will satisfy (5).

Thus, there is a family of solutions that are all equivalent in their decorrelation properties but differ dramatically in their spatio-temporal profiles. The solution that should be selected is the one that satisfies the obvious biological and physical constraints on the problem. For example, since $K(\underline{x}, t)$ is the transfer function of a physical system, it ought to obey the constraint of causality (i.e. $K(\underline{x}, t) = 0$ for $t < 0$). Not all solutions to equation (5) do that. As is shown in Appendix A, imposing the constraint of causality and minimum phase eliminates the temporal phase arbitrariness (up to a constant time delay) and uniquely determines the solution up to a spatial phase $\Phi(\underline{f})$, thus, reduces the size of the family of solutions of (5).

If among this reduced family of solutions one looks for solutions that have no directional bias, *i.e.* even-symmetric solutions ($K(\underline{x}, t) = K(-\underline{x}, t)$) [§], then as shown in Appendix A, there are only two solutions that are allowed, and they are related to each other by overall multiplication of minus sign.

Ideally, this type of cell alone is enough to achieve a decorrelated spatio-temporal representation of natural time-varying images. However, this is true only for a purely linear representation and we know that there are important nonlinearities in the visual pathway leading to the LGN. Next, we examine the effects of these nonlinearities on the predicted LGN coding. We will see that while the nonlinearities do not significantly affect the tuning curves of the cells they do have drastic effects on their response phase and they lead to functional diversity according to phase.

2. Effects of nonlinearities: Lagged and nonlagged cells

Real neurons are not linear units; instead their input-output relationships tend to exhibit significant nonlinearities when the entire range of input signal is considered. For our analysis here, the most relevant feature of this nonlinearity is rectification; *i.e.*, only inputs above certain threshold generate action potentials. Actually, for LGN neurons, two types of rectification have to be taken into account. First, the input to the LGN — which is the retinal output — is rectified and second the LGN output itself is rectified (see Figure 3).

Before we examine the effects of this two stage rectification on the LGN coding we shall make one simplifying assumption, namely, that spatial and temporal decorrelations are done

[§] In general this requirement is less restrictive than rotational symmetry but is equivalent to it if $R(\underline{x}, t)$ is rotationally symmetric.

separately at two different stages along the visual pathway. In other words, we will assume that the output of retinal ganglion cells is fully decorrelated spatially, but that the output of any given ganglion cell still possesses significant correlations over time. The LGN is assumed to fully eliminate these temporal correlations but does nothing in space. In the real visual pathway, this spatio-temporal separation is not exactly true, since ganglion cells attempt to partially decorrelate in time simultaneously with their decorrelation in space. Nevertheless, this is not a bad first approximation since it is clear from the data (Levine and Troy 1986, Victor 1987, Kaplan *et al.* 1993) that in the temporal domain the bandpass filtering of retinal cells is rather flat (and hence not much temporal decorrelation there) compared to the LGN; while in the spatial domain, the LGN cells have receptive fields that are very similar to retinal receptive fields (and hence not much additional spatial processing is performed at LGN). In terms of the input power spectrum, this simplification is also justified since the power spectrum, dominated by motions of objects in visual scenes relative to the observer, is also approximately separable in space and time (Dong and Atick 1994).

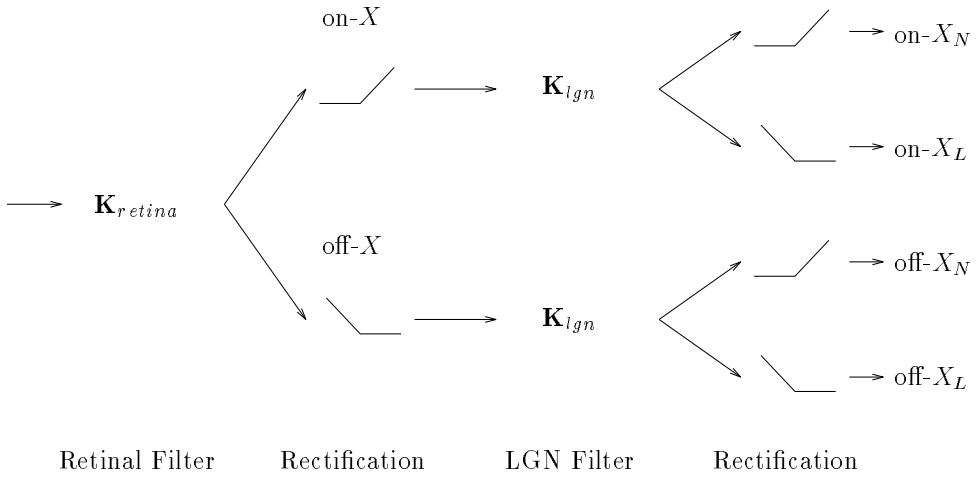

Figure 3: Schematic of the relevant processing stages that we believe the visual input goes through as it emerges from the LGN. In the first stage, the signal is processed by the retinal kernel $\mathbf{K}_{retina}$ to mostly eliminate spatial correlations, it is then rectified to produce the on and off channels which constitute the input to the LGN. The signal is further processed by $\mathbf{K}_{lgn}$ in the LGN to complete its spatio-temporal decorrelation and then rectified. The final result is that there are four cell types: on and off lagged (X_L) and nonlagged (X_N) as indicated.

We should emphasize that the assumption of separability is made for simplification of discussion in this section and is not necessary. In fact, the full and careful treatment of the spatio-temporal decorrelation without this assumption is presented in Appendix B. The results, however, do not deviate significantly from those derived here.

The retinal output, because of rectification, has to come in two varieties, the on and off type given by

$$\mathbf{O}_{\pm} = \pm\mathbf{K}_{retina} \cdot \mathbf{S}\ H(\pm\mathbf{K}_{retina} \cdot \mathbf{S}), \tag{15}$$

in which H is the Heaviside step function:

$$H(x) = \begin{cases} 1, & \text{if } x > 0; \\ 0, & \text{if } x < 0. \end{cases} \tag{16}$$

otherwise the retina loses incoming information.[¶] In this approximation, an on-center

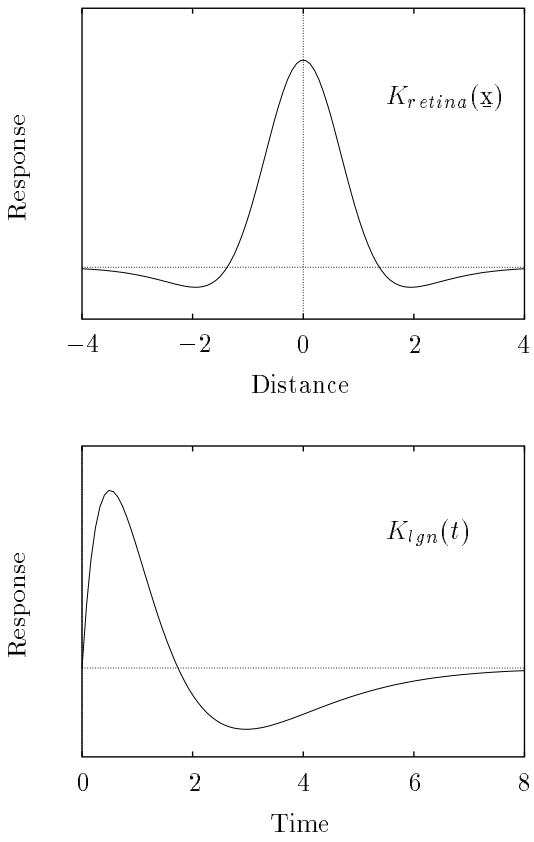

Figure 4: *top:* A cross section of the retinal kernel in space. This kernel was computed to spatially decorrelate incoming images given a small level of noise. The units of distance are in pixels. *bottom:* The kernel that decorrelates natural signals in time, it is given by the analytic formula $K_{lgn}(t) = t(1 - \pi w_c t)e^{-2\pi w_c t}$ where w_c is the characteristic noise cutoff ($w_c = 5.5$ Hz in the plot). This kernel is derived in Appendix A as the optimal solution that decorrelates a signal with power spectrum $1/w^2 + 1/w_c^2$ and it suppresses noise above w_c. The units of time are in increments of 33 ms. Thus the receptive field is about 8 pixels wide and persists in time for more than 200 ms.

neuron responds linearly only when its input is above 0, but it loses information when $\mathbf{K}_{retina} \cdot \mathbf{S}$ is negative. This information is recovered by the off channel such that $\mathbf{O}_+ + (-\mathbf{O}_-) = \mathbf{K}_{retina} \cdot \mathbf{S}$, and hence no information is lost by the combined system. In this section, with the assumption of separability, the retinal kernel $\mathbf{K}_{retina}$ is given simply by:

$$\mathbf{K}_{retina}(\underline{x}, t) = K_{retina}(\underline{x})\delta(t), \tag{17}$$

[¶]In general, cells have thresholds that differ from zero and in detailed comparison with experiments these thresholds may have to be taken into account. For our analysis here we will continue to ignore them for simplicity.

where $K_{retina}(\underline{x})$ is the decorrelating spatial kernel which we computed from spatial properties of natural images; a cross section of this kernel is given in Figure 4-top.

The second source of rectification is at the level of the LGN output. The LGN processes the retinal output $\mathbf{O}_{\pm}$, through a kernel $\mathbf{K}_{lgn}$ which performs the temporal decorrelation of the signal and then rectifies (see Figure 3). In general, the retinal on and off channels could be mixed in the input to the LGN. However, in Appendix B, we find that the mixing is weak in the sense that for any LGN cell either the on or off input dominates. Here, we continue to make the assumption of separability in which case the predicted LGN cell outputs are:

$$\begin{aligned} \mathbf{O}_N &= +\mathbf{K}_{lgn} \cdot \mathbf{O}\ H(+\mathbf{K}_{lgn} \cdot \mathbf{O}), \\ \mathbf{O}_L &= -\mathbf{K}_{lgn} \cdot \mathbf{O}\ H(-\mathbf{K}_{lgn} \cdot \mathbf{O}), \end{aligned} \tag{18}$$

where $\mathbf{O}$ stands for the retinal signal which comes in two varieties given by $\mathbf{O}_+$ or $\mathbf{O}_-$, equation (15), while

$$\mathbf{K}_{lgn}(\underline{x}, t) = K_{lgn}(t)\delta(\underline{x}) \tag{19}$$

with $K_{lgn}(t)$ the temporal decorrelating kernel exhibited in Figure 4-bottom. This kernel is given by the simple analytic formula (35) derived in Appendix A.

Thus for any given retinal output (on or off) there are two types of LGN cells whose output we have labelled as $\mathbf{O}_L$ and $\mathbf{O}_N$ for lagged and nonlagged in anticipation of their response properties which we will exhibit in the next section. To summarize, because of double rectification, there must be four LGN cell types which we denote by: on-center X_N, off-center X_N, on-center X_L, and off-center X_L following the notation of Saul and Humphrey (1990). But we should emphasize that these four types of response are not much different: they all have the same spatial and temporal filters, only have sign flipped and output clipped differently.

Results

We start by calculating the response of the four predicted cell types to a sinusoidally modulated spot stimulus on the central region of the receptive field, *i.e.* $S(\underline{x}, t) = \delta(\underline{x})sin(2\pi f_0 t)$ in which f_0 is the modulation frequency. This is the stimulus used by Saul and Humphrey (1990) to classify LGN cells into four cell types.

Figure 5 helps us to get some insight into what the four cells are coding, in which we compute their response timing (phase) relative to the stimuli of same modulation frequency. In this figure, ϕ is the phase of the response, which is defined as the phase of the Fourier component of frequency f_0 of the output relative to the input signal. The central spot luminance is modulated at $f_0 = 1$ Hz as shown at the bottom of the figure. First we can see that all four cell types are indeed distinct and that those labelled lagged have an excitatory response which is delayed relative to the nonlagged ones. The on-X_N cell fires when the

stimulus is bright and reaches its peak before the peak of the stimulus (thus a phase lead). The on-X_L cell lags behind, fires when the luminance decreases (thus a phase lag). Yet the the off-X_N cell lags further whose firing peaks after the on-X_L and just before the luminance valley. Finally, the off-X_L fires when the luminance increases again. Figure 6 shows the predicted results at three different modulation frequencies. Our Figure 5 and 6 correspond well with the response histograms of nonlagged and lagged X cells in Figure 5 and 6 of Saul and Humphrey (1990).

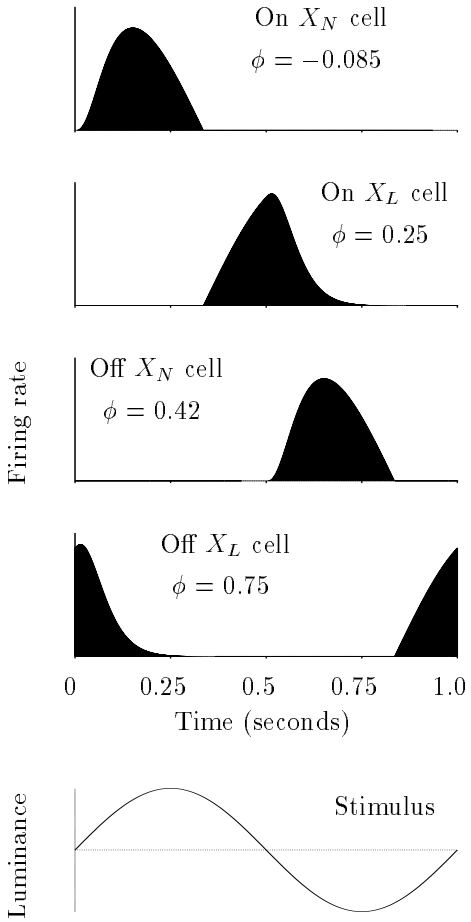

Figure 5: Predicted temporal response of the four cell types to a temporally modulated sinusoidal stimulus at 1 Hz on the receptive field center. ϕ is the phase of the response without propagation delay. The cells labelled X_L are lagged about quarter cycle in their response relative to the X_N cells. The off-X cells are behind corresponding on-X cells by half cycle. This illustrates very clearly the need for the four types of cells and that the on-X_N (X_L) can be thought of as signalling light increment (decrement) when center light level is above surround while off-X_N (X_L) signals light decrement (increment) when center light level is below surround. This figure should be compared with the Figure 5 in Saul and Humphrey (1990). The same $w_c = 5.5$ Hz is used for all the figures except when it is indicated otherwise.

It is clear that the four cell types are necessary if one is not to lose information. This example illustrates the primitive "vocabulary" of the LGN: on-X_N — increment of light

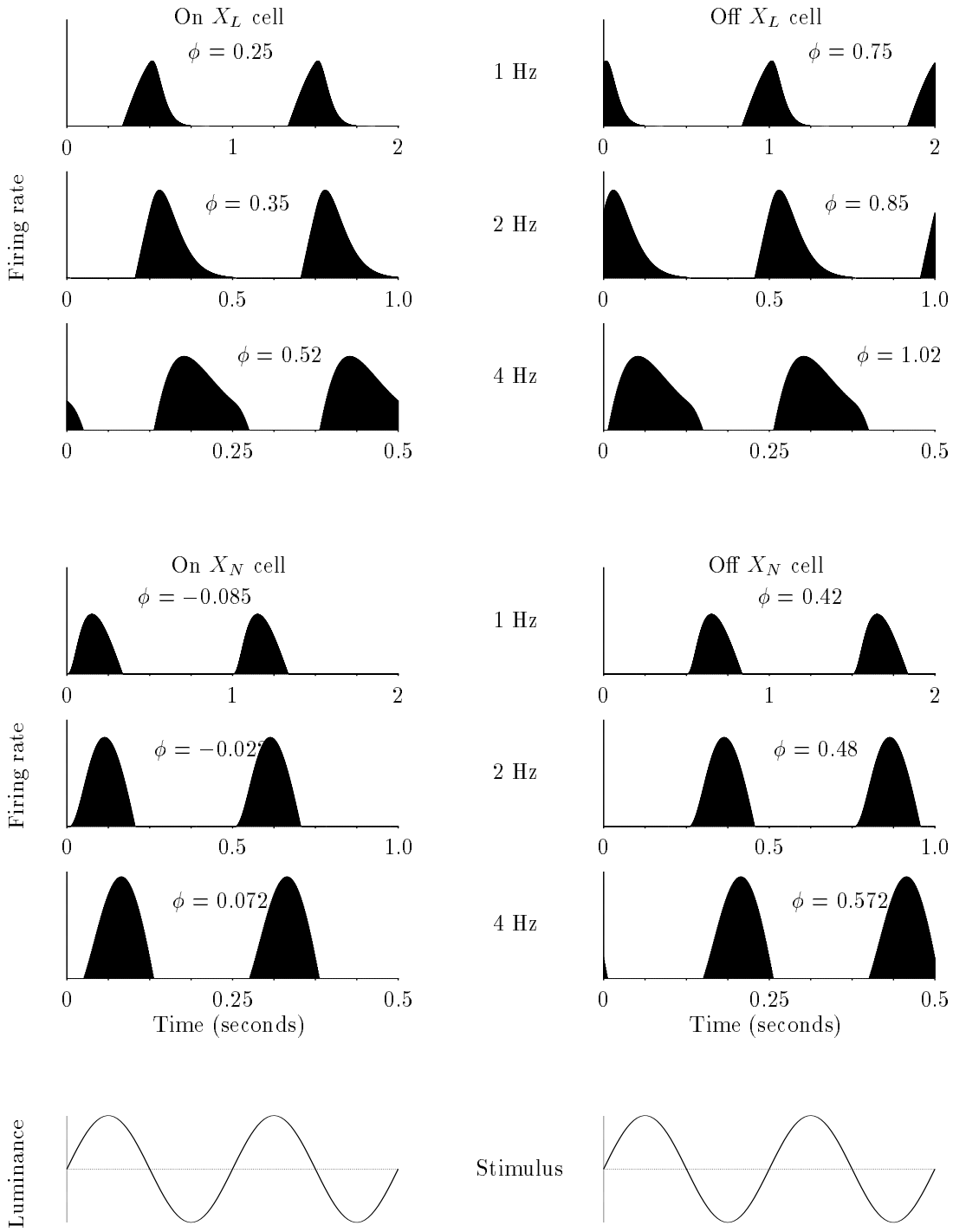

Figure 6: Predicted temporal response of the four cell types to a temporally modulated sinusoidal stimulus at three different frequencies presented on the receptive field center. This shows that the four different cell types have distinct response properties and that cells labelled X_L are lagged in their response relative to the X_N cells. ϕ is the phase of the response without propagation delay. The phase lag of X_L relative to the X_N increases with increasing temporal modulation frequency. The response of the on-X lagged and nonlagged cells in this figure should be compared with the corresponding histograms in Figure 6 in Saul and Humphrey (1990) to see that they indeed correspond well with what is found in experiments.

in center above surround, on-X_L — decrement of light in center above surround, off-X_N — decrement of light in center below surround, and off-X_L — increment of light in center below surround. [‖] This description of the world is complete and is more efficient (*e.g.* signal can be represented by smaller total number of spikes) than signaling the value of light at each frame.

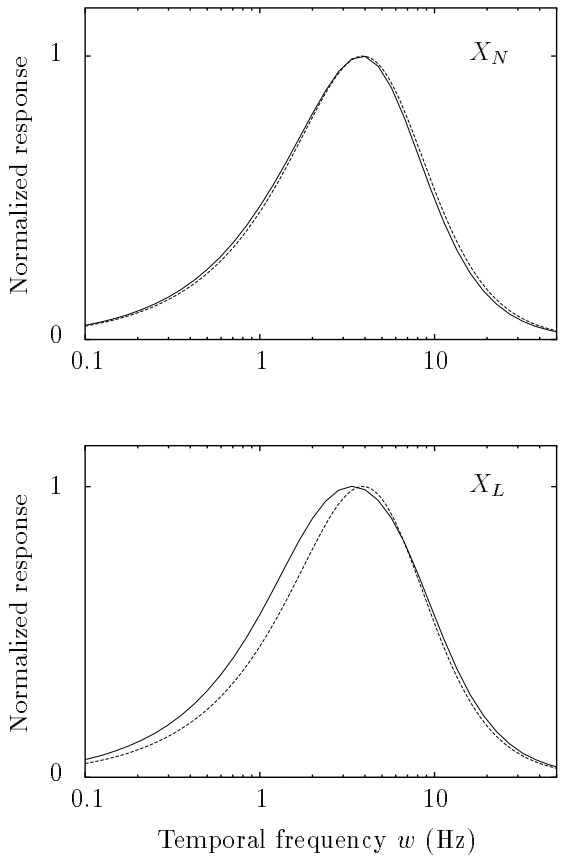

Figure 7: Temporal tuning as computed from the nonlinear theory (solid curves) for nonlagged (*top*) and lagged (*bottom*) cells. For comparison we have also plotted the linear result (dashed curves) as derived from the analytic formula (14). This shows that the linear approximation is not very far from the nonlinear result for the nonlagged cells but that there are significant deviations for the lagged tuning. The most important difference is that the peak is shifted towards smaller frequency for the lagged cells.

In section two we derived analytically the temporal tuning function for LGN cells in the linear approximation. For the nonlinear system, we have computed numerically the tuning curves for X_N and X_L cells. The results are shown in Figure 7, where we have also plotted the analytic result, equation (14), from the linear system for comparison. As we can see from the top figure, the linear result is very close to the true tuning curve for the X_N cells.

[‖] Of course, for the real LGN cells, this notion should be modified a little bit since they do have some level of spontaneous discharge and do not spatially or temporally clip off in a clean-cut fashion. For example, the real on-X_N response extends a little bit on both side of our predict response histogram.

Thus the successes of comparison with the experimental data of Saul and Humphrey (1990) that we achieved in Figure 2 will still be valid for the true nonlinear result. On the other hand, the tuning curve for X_L deviates from the linear result by some small but significant amount. One prediction that this analysis makes is that the peak of the temporal response for a lagged cell is shifted towards smaller frequency relative to that of a nonlagged cell but the overall shapes of their tuning curves are still similar.

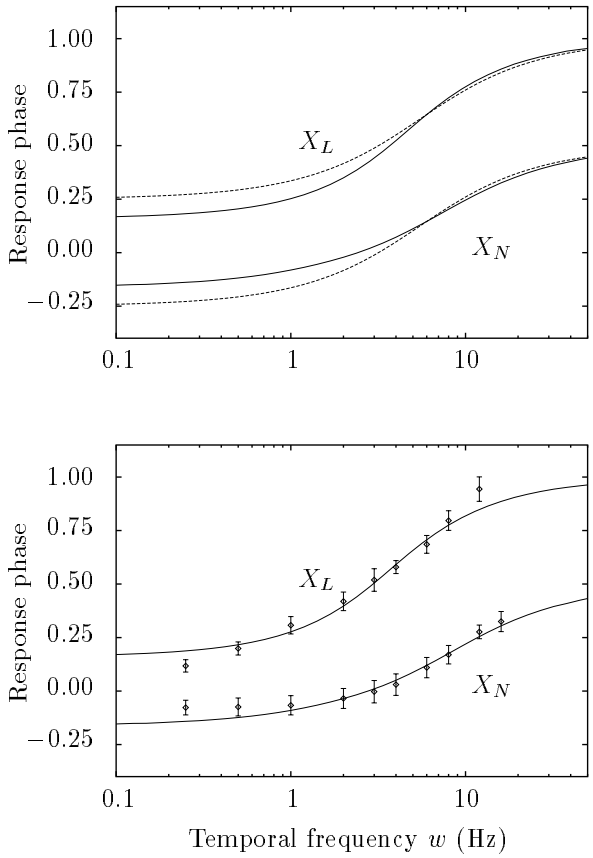

Figure 8: *top:* Predicted response phase, in cycles, for X_L and X_N from the nonlinear theory (solid curves) versus the linear result (dashed line). As shown in Appendix A, the linear theory predicts a phase equation of the form $\phi(w) = \frac{3}{2\pi}\arctan(w/w_c) \pm 1/4$ with $-$ in the second term for nonlagged and $+$ for lagged. *bottom:* Comparison between predicted response phases (solid curves) and the data from Saul and Humphrey (record RF21: cell 04M, 07C, 08P, 03M, 06F, and 09J). The phases are plotted with error bars (averaged over three X_L cells and three X_N cells, respectively). We have taken into account the overall delay from the time when light is presented to the time the signal arrives at the LGN (propagation delay) in the experimental data. Thus the phases plotted are the experimental data minus Tw for a delay time $T = 25$ ms for all cells. In this fit, w_c is 6.3 Hz for X_N and 4.4 Hz for X_L. This is justified since X_L cells have smaller optimal temporal frequency on average (see text).

We have computed the response phase of the lagged and nonlagged cells as a function of temporal frequency. In Appendix B, we derive analytic formulae for the phase of the

response for the nonlagged and lagged cells in the linear approximation. In Figure 8 the numerical results for this phase of response are shown together with the analytic curves. The analytic result deviates significantly from the corresponding nonlinear result mostly at low frequency but in general it is a simple first approximation to the phase. Furthermore, we can see that the relative phase difference between nonlagged and lagged cells increases from quarter cycle at low frequency to half cycle at high frequency. In the bottom portion of this figure we have compared these phases to what is measured by Saul and Humphrey (data provided to us in personal communications). The predictions are definitely consistent with the measurements, especially in the frequency range of 1 to 10 Hz where the tuning curve peaks. We should emphasize that we have taken into account the overall delay from the time when light is presented to the time the signal arrives at the LGN and deducted the phase corresponding this time delay from the experimental data. This typical propagation delay time is the same for all lagged and nonlagged cells.

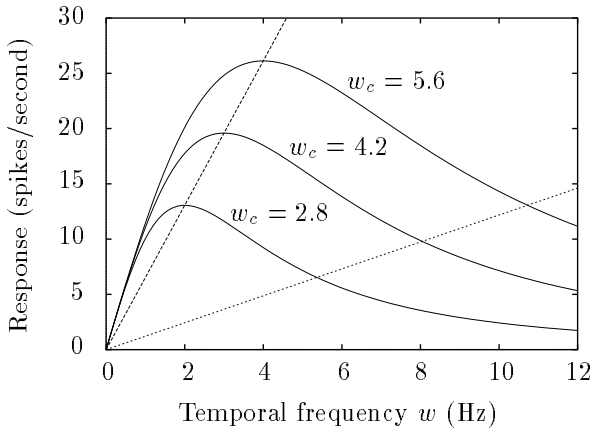

Figure 9: The predicted scaling behaviour of tuning curve for three different w_c (2.8, 4.2, 5.6 Hz, respectively). For higher noise level, thus smaller w_c, the maximal response amplitude and optimal temporal frequency are smaller and scale with w_c; so the peaks of tuning curves lie on a straight line (the dashed line). The scaling also holds for other points on the tuning curve, for example, the half fall points lie on a straight line as well (the dotted line). This cell is the same as in Figure 2 when $w_c = 5.5$ Hz.

Another powerful prediction of our theory is that: everything scales according to a single parameter — w_c which is inversely proportional to the noise level. For example, the maximal response amplitude A_m, optimal temporal frequency w_m, and half fall temporal frequency w_h, are related to w_c simply as follows

$$\begin{aligned} A_m &= A w_c \\ w_m &= \frac{1}{\sqrt{2}} w_c \\ w_h &= 1.9 w_c \end{aligned} \tag{20}$$

in which A is independent of noise level. If a cell is adapted to different noise level, thus different w_c, its tuning curve will just scale accordingly. The theoretical prediction of scaling

behaviour is illustrated in Figure 9. We see that when the noise level becomes higher, the tuning curve shifts to lower temporal frequency, thus the responses to higher frequencies decrease significantly whereas the responses to lower frequencies do not change much.** This scaling behaviour could be partially true for a population of cells if they were similar cells and had similar signal inputs but had different noise levels.†† The response phase scales with w_c as well. For different w_c, the phase curves will be the same if the temporal frequency is plotted in unit of w_c. There are not enough data available to fully test this at present time. We are looking forward to new experimental results to compare with our theoretical predictions.

Discussion

At this moment, it is not entirely clear whether nonlagged and lagged responses represent different cell classes (Mastronarde 1987a,b; Humphrey and Weller, 1988) or different response modes of the same cells (Uhlrich *et al.* 1990) or both. Either interpretation is consistent with the predictions of efficient coding, since efficiency dictates the need for lagged and nonlagged "responses" without specifying how these should be accomplished. Although we have used the terminology lagged and nonlagged "cells" for concreteness throughout the paper, it should be understood that we really mean "responses".

We need to emphasize that what we presented in this paper is only the first step towards a complete theory of the LGN function. After all, the LGN receives massive feedback from the cortex and the brain stem and the computational purpose of such feedback has to be accounted for by the theory. This feedback is known to alter the temporal properties of lagged and nonlagged cells depending on certain conditions such as the state of arousal of the animal (Uhlrich *et al.* 1990; Humphrey and Saul 1992; Hartveit and Heggelund 1993; Kaplan et al. 1993). While at the moment our theory does not include this feedback, there are some very tantalizing results about its computational purpose that emerge from closer examination of the principle of efficient coding in the presence of noise.

Generally speaking, we believe the feedback controls the degree of temporal decorrelation of the signal. The need to do this is a consequence of the fact that, in the presence of noise, efficient coding requires decorrelation where the signal is strong and smoothing where noise is significant. Under the earlier condition the LGN needs to decorrelate more while under the latter the LGN needs to decorrelate less. The end result is that by chosing the correct

**For real neurons which are not entirely transient, i.e., their responses contain DC components, such shift will change the tuning curve from bandpass to lowpass filter. Of course, the scaling will only hold approximately in that case.

††The average w_m and A_m of X_L cells are smaller than those of X_N cells by roughly the same factor (Table 2, Saul and Humphrey 1990). If the lagged cells were more noisy than the nonlagged cells, it would be a confirmation of our scaling prediction.

degree of decorrelation the signal is compressed by elimination of what is irrelevant without significant loss of information.

In this way of looking at things, the feedback must be signalling to the LGN what it should treat as "noise" and what it should treat as "signal". Noise is then not just quantum noise or other intrinsic fluctuations in the input but is also what the animal — in a given state of "adaptation" — should consider as irrelevant. This certainly depends on the state of arousal or the behavioral state of the animal and involves higher processing. However, once the signature of "noise" is given, the system can adapt to achieve the degree of bandpass filtering desired (or equivalently, the degree of lowpass filtering). We intend to explore such dynamic theory of the LGN in a future publication.

Actually, the idea that the feedback plays the role of a gain control which gates the information flow through the LGN is not new; it was proposed earlier by several groups (Singer 1977; Crick 1984; Harth and Unnikrishnan 1985; Sherman and Koch 1986). What is new here is the suggestion that the gating is accomplished through controlling the degree of temporal decorrelation of the signal.

Another limitation of the analysis presented here is that it deals only with the so called X cells which, apart from rectification, linearly integrate signals over their receptive fields. The other cell variety known in the cat LGN (and retina), the Y cells, exhibit significant nonlinearities even in regimes where the X cells linearize. At the moment we do not have a predictive theory of Y cell coding neither in space nor in time. There are some other suggestions about the different roles of X and Y cells in temporal information processing (*e.g.* Van Essen and Anderson 1990; Li 1992) but none have made quantitative predictions or have explained the lagged and nonlagged cell types in LGN.

Finally, it was previously suggested that lagged and nonlagged cells in the LGN provide the building blocks for directionally selective simple cells and that this may be the fundamental reason why such functional diversity exists in the LGN (Saul and Humphrey 1990). In fact there is now evidence showing that some simple cells in area 17 receive inputs from both lagged and nonlagged LGN cells (Saul and Humphrey 1992). While we fully agree that the outputs of lagged and nonlagged cell pairs are well suited for building in a simple way directionally selective units at the next stage we do not believe this is the primary reason functional diversity exists in the LGN. Generally speaking, efficient representations can be argued to simplify the computations involved in a multitude of cognitive tasks not just direction selectivity and besides by adopting efficiency as the underlying principle we are able to use properties of natural signals to make quantitative predictions, which is ultimately what a theory is about.

Acknowledgements

We wish to acknowledge Ehud Kaplan, Clay Reid, and Corinna Darian-Smith for very helpful conversations and Alan Saul for kindly supplying us with some of his data. We are especially indebted to Clay Reid for showing us the cell diversity in his LGN data which stimulated our thinking about the computational role of the LGN. This work is supported in part by the Seaver Institute.

Appendix A: Causality & Analytic Solutions

In this appendix we show how to construct the causal solution to Equation (5) and illustrate the procedure by applying it in the limit of zero spatial frequency (where closed form formula for $R(0,w)$ exists) to derive analytic formulas for $K(w)$, $\phi(w)$ and $K(t)$.

The Weiner-Hopf Technique

In general, the principle of efficient coding leads to an equation for the filter $K(\underline{f},w)$ of the form:

$$K(\underline{f},w)\ K(\underline{f},w)^* = Q(\underline{f},w) \tag{21}$$

for some function $Q(\underline{f},w)$ that is determined by the statistics of natural scenes and noise statistics. In the limit where noise is negligible, as is shown in section two, $Q(\underline{f},w) = 1/R(\underline{f},w)$. More generally, when noise is not negligible $Q(\underline{f},w) = (R(\underline{f},w) - N^2)^2/R(\underline{f},w)^3$. In the absence of additional constraints, the solution to equation (21) for $K(\underline{f},w)$ is not unique, since the equation does not determine the phase of the solution.

It is clear that not all solutions of (21) are physical. For example, we can only accept solutions that are causal; the cell cannot respond before the on-set of the stimulus and thus we need solutions that satisfy $K(\underline{x},t) = 0$ for $t < 0$. To construct causal solutions we use Weiner-Hopf spectrum factorization (Lee 1960). As we prove next, the requirement of causality of $log(K(\underline{f},w))$ reduces the arbitrariness to phase functions that are independent of temporal frequency. ‡‡

We start by taking the logarithm of equation (21) to arrive at

$$\begin{aligned} log(K(\underline{f},w)) + log(K^*(\underline{f},w)) &= log(Q(\underline{f},w)) \\ &\equiv \mathcal{F}(\underline{f},w) \end{aligned} \tag{22}$$

‡‡The constraint of causality of $log(K(\underline{f},w))$ is more stringent than causality of $K(\underline{f},w)$. However it is equivalent to a causal filter of minimum phase (Bode 1945). Interestingly, in mammalian auditory systems, the basilar membrane transfer function is also of minimum phase (Zweig 1976). The advantage of minimum phase transfer function in sensory systems is obvious: the response has minimum time delay after stimuli onset.

the inverse Fourier transform in time of $\mathcal{F}(\underline{f}, w) = log(Q(\underline{f}, w))$ is $\mathcal{F}(\underline{f}, t)$ and can be decomposed into the sum of causal and anti-causal parts:

$$\mathcal{F}(\underline{f}, t) = \mathcal{F}_+(\underline{f}, t) + \mathcal{F}_-(\underline{f}, t), \tag{23}$$

in which the causal part $\mathcal{F}_+(\underline{f}, t)$ is simply

$$\mathcal{F}_+(\underline{f}, t) = \begin{cases} \mathcal{F}(\underline{f}, t), & \text{if } t > 0; \\ 0, & \text{if } t < 0. \end{cases} \tag{24}$$

and similarly for the anticausal part $\mathcal{F}_-(\underline{f}, t)$.

Transforming $\mathcal{F}_+(\underline{f}, t)$ and $\mathcal{F}_-(\underline{f}, t)$ into Fourier space, they satisfy $\mathcal{F}(\underline{f}, w) = \mathcal{F}_+(\underline{f}, w) + \mathcal{F}_-(\underline{f}, w)$. So

$$log(K(\underline{f}, w)) + log(K^*(\underline{f}, w)) = \mathcal{F}_+(\underline{f}, w) + \mathcal{F}_-(\underline{f}, w) \tag{25}$$

Since $log(K(\underline{f}, w))$ and $F_+(\underline{f}, w)$ are both causal, and $log(K^*(\underline{f}, w))$ and $F_-(\underline{f}, w)$ are anti-causal we are led to the following solutions:

$$\begin{aligned} log(K(\underline{f}, w)) &= \mathcal{F}_+(\underline{f}, w) + \Theta(\underline{f}) \\ log(K^*(\underline{f}, w)) &= \mathcal{F}_-(\underline{f}, w) - \Theta(\underline{f}), \end{aligned} \tag{26}$$

in which $\Theta(\underline{f})$ is any function independent of w. The desired causal solution is determined by

$$K(\underline{f}, w) = e^{\Phi(\underline{f})}\ e^{\mathcal{F}_+(\underline{f}, w)} \tag{27}$$

Thus by imposing the constraint of causality of $log(K(\underline{f}, w))$ we have reduced the arbitrariness in the solution $\mathbf{K}$ to a choice of spatial phase. To fix the choice of spatial phase we impose the condition that $K(\underline{x}, t)$ is a real and even function of $\underline{x}$, $K(\underline{x}, t) = K(-\underline{x}, t)$ (less restrictive than rotational symmetry but equivalent to it if $R(\underline{x}, t)$ of natural scenes is rotationally symmetric). These constraints are equivalent to

$$K^*(\underline{f}, w) = K(-\underline{f}, -w) = K(\underline{f}, -w). \tag{28}$$

which, through equation (26), leads to

$$exp(\mathcal{F}_+(\underline{f}, -w) + \Theta(\underline{f})) = exp(\mathcal{F}_-(\underline{f}, w) - \Theta(\underline{f})). \tag{29}$$

For a physical real system the relationship $F_+(\underline{f}, t) = F_-(\underline{f}, -t)$ is true and thus

$$F_+(\underline{f}, -w) = F_-(\underline{f}, w) \tag{30}$$

which means that the only allowed phases that are consistent with the constraint of even-symmetry are those which satisfy:

$$e^{2\Theta(\underline{f})} = 1 \quad , \tag{31}$$

which has only two solutions $\Theta(\underline{f}) = 0$ or $\Theta(\underline{f}) = i\pi$ corresponding to an overall multiplication by a plus or minus sign.

Example

As shown in section two, in the limit of zero spatial frequency, the principle of efficient coding (taking noise into account) gives the following equation for $K(\underline{f}, w)$

$$K(\underline{f}, w)\ K(\underline{f}, w)^* = \frac{w^2}{(1 + (w/w_c)^2)^3} \tag{32}$$

in which w_c is a cutoff proportional to the noise power.

Following the factorization procedure above, it can be shown that

$$K(w) = \frac{-iw}{(1 - iw/w_c)^3}, \tag{33}$$

which means that the response function is given by (14) and the phase, in units of cycles, is

$$\phi(w) = \frac{3}{2\pi} \arctan(w/w_c) - \frac{1}{4}, \tag{34}$$

while the temporal kernel is

$$K(t) = t(1 - \pi w_c t)e^{-2\pi w_c t}. \tag{35}$$

The kernel (35) is plotted in Figure 4-bottom and the phase function is exhibited in Figure 8-top; the lagged phase response is related to the nonlagged phase through a shift by π. As is shown in section four, these simple analytic formulae provide good first order approximations to the cell response properties.

Appendix B: Spatio-Temporal Inseparability

In section three we have made the simplifying assumption that retinal cells do not perform any significant temporal processing and that they merely decorrelate in space and the LGN cells merely decorrelate in time. This is not exactly true in the real visual pathway. The correct thing to do is to allow the retinal cells to filter the natural input and then study the statistics of the retinal output after rectification. Then use this spatio-temporal statistics to predict kernels which fully decorrelate in both space and time the retinal signal.

The general problem is as follows. The LGN receives signals from on and off channels in the retina. Those signals have temporal correlations and perhaps some residual spatial correlations. We should allow for the possibility that there is some small correlation between the on and off channels. To decorrelate, the LGN must choose a kernel, $\mathbf{K}$ that diagonalizes the correlation matrix of retinal outputs $\mathcal{R}$:

$$\mathbf{K} \cdot \mathcal{R} \cdot \mathbf{K}^T = 1 \ , \tag{36}$$

Since there are two types of input cells, the on and off, the above equation can be written more explicitly as:

$$\begin{pmatrix} \mathbf{K}_{1+} & \mathbf{K}_{1-} \\ \mathbf{K}_{2+} & \mathbf{K}_{2-} \end{pmatrix} \begin{pmatrix} \mathbf{r} & \mathbf{q} \\ \mathbf{q} & \mathbf{r} \end{pmatrix} \begin{pmatrix} \mathbf{K}_{1+} & \mathbf{K}_{1-} \\ \mathbf{K}_{2+} & \mathbf{K}_{2-} \end{pmatrix}^T = \mathbf{1}, \tag{37}$$

in which $\mathbf{r} =< \mathbf{O}_+\mathbf{O}_+ >=< \mathbf{O}_-\mathbf{O}_- >$ and $\mathbf{q} =< \mathbf{O}_-\mathbf{O}_+ >=< \mathbf{O}_+\mathbf{O}_- >$ where $\mathbf{O}_\pm$ is the retinal output and where we have made the assumption of symmetry of the on and off channels.

In order to solve the above equation, we first perform a transformation to the principal axes of the covariance matrix by rotating in the on-off space by

$$\frac{1}{\sqrt{2}} \begin{pmatrix} 1 & -1 \\ 1 & 1 \end{pmatrix}, \tag{38}$$

i.e., rotation into the base of $(\mathbf{O}_+ - \mathbf{O}_-)$ and $(\mathbf{O}_+ + \mathbf{O}_-)$. In this basis, the correlation matrix becomes

$$\frac{1}{2} \begin{pmatrix} 1 & -1 \\ 1 & 1 \end{pmatrix} \begin{pmatrix} \mathbf{r} & \mathbf{q} \\ \mathbf{q} & \mathbf{r} \end{pmatrix} \begin{pmatrix} 1 & 1 \\ -1 & 1 \end{pmatrix} = \begin{pmatrix} \mathbf{R}_- & 0 \\ 0 & \mathbf{R}_+ \end{pmatrix} \quad , \tag{39}$$

which is block diagonal, and in which $\mathbf{R}_\pm = \mathbf{r} \pm \mathbf{q}$.

Next, we find $\mathbf{K}_-$ and $\mathbf{K}_+$ which satisfy $\mathbf{K}_\pm \cdot \mathbf{R}_\pm \cdot \mathbf{K}_\pm^T = \mathbf{1}$ as we have done in section two. The final solution (transforming back into the original coordinate base) is

$$\begin{pmatrix} \mathbf{K}_{1+} & \mathbf{K}_{1-} \\ \mathbf{K}_{2+} & \mathbf{K}_{2-} \end{pmatrix} = \frac{1}{2} \begin{pmatrix} \mathbf{K}_+ + \mathbf{K}_- \ , & \mathbf{K}_+ - \mathbf{K}_- \\ \mathbf{K}_+ - \mathbf{K}_- \ , & \mathbf{K}_+ + \mathbf{K}_- \end{pmatrix}. \tag{40}$$

Now there are two cell types

$$\begin{aligned} \mathbf{O}_1 &= (\mathbf{K}_+ + \mathbf{K}_-) \cdot \mathbf{O}_+ + (\mathbf{K}_+ - \mathbf{K}_-) \cdot \mathbf{O}_- \\ \mathbf{O}_2 &= (\mathbf{K}_+ + \mathbf{K}_-) \cdot \mathbf{O}_- + (\mathbf{K}_+ - \mathbf{K}_-) \cdot \mathbf{O}_+ \end{aligned} \tag{41}$$

where $\mathbf{O}_\pm$ are the retinal outputs computed using the most accurate rectified spatio-temporal retinal on and off kernels. The outputs $\mathbf{O}_1$ and $\mathbf{O}_2$ when rectified lead to four cell types. Rectification of $\mathbf{O}_1$ ($\mathbf{O}_2$) leads to on-center (off-center) lagged and nonlagged cells. We see that the contribution of the off-center retinal channel to an on-center LGN cell is proportional to the $\mathbf{K}_+ - \mathbf{K}_-$ which is much smaller than the contribution of the on-center retinal channel $(\mathbf{K}_+ + \mathbf{K}_-)$ and hence the classification into on and off channels should still persist in the LGN.

Using a more realistic spatio-temporal retinal filter derived from various experiments, similar to the one used in Wehmeier *et al.* (1989), we have calculated the correlation matrix of retinal responses, $\mathcal{R}$, to the same set of time-varying images used to derive $R(\underline{f}, w)$, and then numerically evaluated the response properties of cells computed from the above result. We found only minor modifications to the response properties computed under the simplifying assumptions of section three. Thus, with the current reliability level of data, there is no reason to use anything more complicated than the simple results of section three.

References

[1] Atick JJ (1992a) Entropy minimization: a design principle for sensory perception. Int J of Neural Systems 3: 81–90.

[2] Atick JJ (1992b) Could information theory provide an ecological theory of sensory processing? Network: Computations in Neural Systems 3: 213–251.

[3] Atick JJ, Redlich AN (1990) Towards a theory of early visual processing. Neural Comp 2: 308–320.

[4] Atick JJ, Redlich AN (1992) What does the retina know about natural scenes? Neural Comp 4: 196–210.

[5] Atick JJ, Li Z, Redlich AN (1992) Understanding retinal color coding from first principles. Neural Comp 4: 559–572.

[6] Atick JJ, Li Z, Redlich AN (1993) What does post-adaptation color appearance reveal about cortical color representation. Vision Res 33: 123–129.

[7] Attneave F (1954) Some informational aspects of visual perception. Psychol Rev 61: 183–193.

[8] Barlow HB (1961) Possible principles underlying the transformation of sensory messages. In: Sensory Communication (Rosenblith WA, ed). Cambridge, MA: MIT Press.

[9] Barlow HB (1989) Unsupervised learning. Neural Comp 1: 295–311.

[10] Bode H (1945) Network Analysis and Feedback Amplifier Design. Princeton, NJ: Van Nostrand Reinhold.

[11] Cleland BG, Dubin MW, Levick WR (1971) Sustained and transient neurons in the cat's retina and lateral geniculate nucleus. J Physiol (Lond) 217: 473–496.

[12] Crick F (1984) Function of the thalamic reticular complex: the searchlight hypothesis. Proc. Natl. Acad. Sci. USA 81: 4586–4590.

[13] Dong DW (1993a) Anti-Hebbian dynamics and total recall of associative memory. Proc World Congress on Neural Networks, Portland. (Hillsdale, NJ: Erlbaum) 2: 275–279.

[14] Dong DW (1993b) Associative decorrelation dynamics in visual cortex. Lawrence Berkeley Laboratory Technical Report. LBL-34491.

[15] Dong DW (1994) Associative decorrelation dynamics: a theory of self-organization and optimization in feedback networks. In: Advances in Neural Information Processing Systems 7 (Tesauro G, Touretzky DS, Leen TK, eds). Cambridge, MA: MIT Press. 925–932.

[16] Dong DW, Atick JJ (1994a) Temporal decorrelation: a theory of lagged and nonlagged responses in the lateral geniculate nucleus (LGN). Society for Neuroscience Abstract 20: 7.

[17] Dong DW, Atick JJ (1995) Statistics of natural time varying images. Submitted to the *Network*.

[18] Field DJ (1987) Relations between the statistics of natural images and the response properties of cortical cells. J Opt Soc Am A 4: 2379–2394.

[19] Hancock PJB, Baddeley RJ, Smith LS (1992) The principal components of natural images. Network: Computation in Neural Systems 3: 61–70.

[20] Harth E, Unnikrishnan KP (1985) Brainstem control of sensory information: A mechanism for perception. Int J of Psychophys 3:101–119.

[21] Hartveit E (1992) Simultaneous recording of lagged and nonlagged cells in the cat dorsal lateral geniculate-nucleus. Exp Brain Res 88: 229–232.

[22] Hartveit E, Heggelund P (1993) Brain-stem influence on visual response of lagged and nonlagged cells in the cat lateral geniculate-nucleus. Vis Neuros 10: 325–339.

[23] Hubel DH, Wiesel TN (1961) Integrative action in the cat's lateral geniculate body. J Physiol (London) 155: 385–398.

[24] Humphrey AL, Saul AB (1992) Action of brain-stem reticular afferents on lagged and nonlagged cells in the cat lateral geniculate-nucleus. J Neurophysiol 68: 673–691.

[25] Humphrey AL, Weller RE (1988) Functionally distinct groups of X-cells in the lateral geniculate nucleus of the cat. J Comp Neurol 268: 448–468.

[26] Kaplan E, Mukherjee P, Shapley RM (1993) Information filtering in the lateral geniculate nucleus. In: Contrast Sensitivity (Shapley RM, Lam D, eds), pp 183–200. Cambridge: MIT Press.

[27] Kaplan E, Shapley R (1982) What controls information processing in the LGN? Society for Neuroscience Abstract 8: 405.

[28] Lee YW (1960) Statistical Theory of Communication. New York, NY: John Wiley.

[29] Levine MW, Troy JB (1986) The variability of the maintained discharge of cat dorsal lateral geniculate cells. J Physiol (Lond) 375: 219–246.

[30] Li Z (1992) Different retinal ganglion cells have different functional goals. Int J of Neural Systems. 3: 237–248.

[31] Li Z, Atick JJ (1994) Efficient stereo coding in the multiscale representation. Network: Computations in Neural Systems 5: 1–18.

[32] Linsker R (1989) An application of the principle of maximum information preservation to linear systems. In: Advances in Neural Information Processing Systems 1 (Touretzky DS, ed), pp. 186–194. San Mateo, CA: Morgan Kaufman.

[33] Mastronarde DN (1987a) Two classes of single-input X-cells in cat lateral geniculate nucleus. I. Receptive-field properties and classification of cells. J Neurophysiol 57: 357–380.

[34] Mastronarde DN (1987b) Two classes of single-input X-cells in cat lateral geniculate nucleus. II. Retinal inputs and the generation of receptive-field properties. J Neurophysiol 57: 381–413.

[35] Press WH, Flannery BP, Teukolsky SA, Vetterling, WT (1988) Numerical Recipes: the Art of Scientific Computing. Cambridge: Cambridge Press.

[36] Ruderman DL, Bialek W (1994) Statistics of natural images: Scaling in the woods. In: Advances in Neural Information Processing Systems 6 (Cowan JD, Tesauro G, Alspector J, eds). San Fancisco: Morgan Kaufman.

[37] Saul AB, Humphrey AL (1990) Spatial and temporal response properties of lagged and nonlagged cells in cat lateral geniculate-nucleus. J of Neurophysiol 64 : 206–224.

[38] Saul AB, Humphrey AL (1992) Evidence of input from lagged cells in the lateral geniculate- nucleus to simple cells in cortical area 17 of the cat. J of Neurophysiol 68 : 1190–1208.

[39] Sherman SM, Koch C (1986) The control of retinogeniculate transmission in the mammalian lateral geniculate nucleus. Exp Brain Res 63: 1–20.

[40] Singer W (1977) Control of thalamic transmission by corticofugal and ascending reticular pathways in the visual system. Phys Reviews 57: 386–420.

[41] Singer W, Creutzfeldt OD (1970) Reciprocal lateral inhibition of on- and off-center neurons in the lateral geniculate body of the cat. Exp Brain Res 10: 311–330.

[42] So YT, Shapley R (1979) Spatial properties of X and Y cells in the lateral geniculate nucleus of the cat and conduction velocities of their inputs. Exp Brain Res 36: 533–550.

[43] Uhlrich, D. J., Tamamaki, N. and Sherman, S. M. 1990. Brainstem control of response modes in neurons of the cat's lateral geniculate nucleus. *Proc. Natl. Acad. Sci. USA*, **87**:2560–2563.

[44] Van Essen DC, Anderson CC (1990) Information processing strategies and pathways in the primate retina and visual cortex. In: Introduction to Neural and Electronic Networks (Zotnetzer SF, Davis JL, Lau C, eds) Florida: Academic Press.

[45] Victor JD (1987) The dynamics of the cat retinal X cell centre. J Physiol (Lond) 386: 219–246.

[46] Wehmeier U, Dong DW, Koch C, Van Essen DC (1989) Modeling the mammalian visual system. In: Methods in Neuronal Modeling: from Synapses to Networks (Koch C, Segev I, eds) pp. 335–360. Cambridge, MA: MIT Press.

[47] Zweig G (1976) Basilar Membrane Motion. In: Cold Spring Harbor Symposia on Quantitative Biology 6: 619-633. Cold Spring Harbor Laboratory.